ELSEVIER

Journal of Molecular Catalysis A: Chemical 151 (2000) 205–216

JOURNAL OF MOLECULAR CATALYSIS A: CHEMICAL

www.elsevier.com/locate/molcata

The preparation, characterization, photoelectrochemical and photocatalytic properties of lanthanide metal-ion-doped TiO_2 nanoparticles

Yanqin Wang, Humin Cheng *, Li Zhang [1], Yanzhong Hao, Jiming Ma, Bin Xu, Weihua Li [1]

Department of Chemistry, Peking University, Beijing 100871, China

Received 4 February 1999; received in revised form 6 April 1999; accepted 25 May 1999

Abstract

Lanthanide metal-ion-doped TiO_2 nanoparticles were prepared with hydrothermal method and characterized with X-ray diffraction (XRD), transmission electron microscopy (TEM), inductively coupled plasma (ICP) and fluorescence spectrum. The results showed that a small part of metal ions entered into the lattice of TiO_2 and others adsorbed on the surface of TiO_2. The photoelectrochemical and photocatalytic properties of these lanthanide metal-ion-doped TiO_2 nanoparticles were investigated and the results showed that the photoresponse of Eu^{3+}-, La^{3+}-, Nd^{3+}- and Pr^{3+}-doped TiO_2 electrodes were much larger and that of Sm^{3+}-doped TiO_2 electrode was a little larger than that of undoped TiO_2 electrode, indicating that the photogenerated carriers were separated more efficiently in Eu^{3+}-, La^{3+}-, Nd^{3+}- and Pr^{3+}-doped TiO_2 nanoparticles than in undoped TiO_2 nanoparticles. The photocatalytic degradation of rhodamine B (RB) was conducted in the suspension of lanthanide metal-ion-doped TiO_2 nanoparticles, and its first-order reaction rate constant (k) and average initial rate (r_{ini}) were significantly higher in the presence of Eu^{3+}-, La^{3+}-, Nd^{3+}- and Pr^{3+}-doped TiO_2 nanoparticles than those in the presence of undoped TiO_2 nanoparticles. The enhanced photocatalytic degradation rate of RB in the presence of Eu^{3+}-, La^{3+}-, Nd^{3+}- and Pr^{3+}-doped TiO_2 nanoparticles is attributed to increased charge separation in these systems. The effect of the content of La^{3+} on the reaction parameters (k and r_{ini}) was also investigated and the result showed that there was an optimal value (ca. 0.5%) of the content of La^{3+} to make the rate constant (k) and average initial rate (r_{ini}) reach the maxima.

Keywords: Metal-ion-doped TiO_2 nanoparticles; IPCE; Reactivity; Photocatalytic degradation

1. Introduction

Photocatalytic degradation of several organic contaminants using large bandgap semiconductor particles (such as TiO_2, ZnO, WO_3) have been studied extensively [1–6]. In a slurry-based photocatalytic reactor system, the rate-determining step in the degradation process is considered to be

* Corresponding author. E-mail: wyq@pubms.pku.edu.cn

[1] Scholar from Suzhou Shizhuan.

1381-1169/00/$ - see front matter
PII: S1381-1169(99)00245-9

the reduction of oxygen by trapped electrons on the semiconductor surface to produce reduced oxygen species such as the superoxide radical ion O_2^- or H_2O_2 [6] — these superoxide species have strong oxidizability. Photogenerated electron-hole pairs can also recombine; therefore, suppressing the recombination of electron-hole pairs and prolonging the lifetime of carriers are essential for improving the efficiency of net charge transfer at the semiconductor/electrolyte interface. The work extensively studied previously is to combine together two different semiconductors which have different bandgaps in order to improve the separation efficiency of carriers. These composite systems include CdS/TiO_2 [7], CdS/PbS [8], CdS/ZnO [9], ZnO/ZnS [10], ZnO/TiO_2 [11] and SnO_2/TiO_2 [6], etc.

As to metal-ion-doped TiO_2 powders, Fe^{3+}- and Cr^{3+}-doped TiO_2 powders were studied extensively [12–15] with the purpose of extending the absorption spectrum to visible light. But the results were often controversial; some reports showed that the photooxidativity and photoreducibility were improved through doping, but the other reports showed that the photooxidativity and photoreducibility were reduced. The preparation of lanthanide-ion-doped TiO_2 nanoparticles, as well as their photoelectrochemical and photocatalytic properties, were never reported until now. The reason may be that the absorption spectrum cannot be extended to visible light by doping lanthanide metal ions. Our experimental results showed that lanthanide-ion-doped TiO_2 nanoparticles showed higher photoresponse and higher reactivity for the photocatalytic degradation of rhodamine B (RB) than undoped TiO_2 nanoparticles.

As an important representative of xanthene dyes, RB is famous for its good stability as dye laser materials. Zhang et al. [16], Qu et al. [17] and Wu et al. [18] have studied the mechanism of photocatalytic degradation of RB in the UV and visible light.

In this paper, lanthanide ion (Nd^{3+}, Eu^{3+}, La^{3+}, Sm^{3+} and Pr^{3+})-doped TiO_2 were prepared with hydrothermal method and characterized with X-ray diffraction (XRD), transmission electron microscopy (TEM), atomic force microscopy (AFM), inductively coupled plasma (ICP), fluorescence spectra, and their photoelectrochemical properties were also studied. Photocurrent action spectra and photocurrent–electrode potential curves showed that the photoresponse of lanthanide-ion-doped TiO_2 nanocrystalline electrodes were much larger than that of undoped TiO_2 nanocrystalline electrode in UV-light scale, indicating that photogenerated electron-hole pairs were separated more efficiently in lanthanide-ion-doped TiO_2 nanoparticles. The photocatalytic degradation of RB was carried out in the suspension of lanthanide metal-ion-doped TiO_2 nanoparticles in UV light. As a comparison, the reaction was also carried out in the suspension of undoped TiO_2 nanoparticles. The effect of the content of La^{3+} on the reactivity of photocatalysis of doped TiO_2 nanoparticles was also studied.

2. Experimental procedure

2.1. The synthesis of metal-ion-doped TiO_2 nanoparticles

The TiO_2 nanoparticles were prepared with hydrothermal method which was reported elsewhere [19]. Metal-ion-doped TiO_2 nanoparticles were prepared according to the same procedure in the presence of added metal salt to give an initial doping level of 5% except Nd^{3+} whose molar content was 0.5%. Metal salts used as precursors for doping ions are listed as follows: $La(NO_3)_3$, $Eu(NO_3)_3$, $Nd(NO_3)_3$, $Pr(NO_3)_3$ and $Sm(NO_3)_3$. The pH of the reaction media was controlled at 1.8 except for investigating the effect of the content of La^{3+} on photocatalysis where the nanoparticles were prepared at pH 7.0 with different contents of La^{3+}.

2.2. Characterization of metal-ion-doped TiO_2 nanoparticles

The phase of the reaction products was analyzed by XRD which uses a Cu Kα radiation at 40 kV, 100 mA with a graphite monochromator and scans at 4° min^{-1} (2θ) with a diffractometer (Model Rigku max-2000). A TEM (Model JEM-200CX) was used to characterize the morphology and particle size. The element analysis was carried out by inductively coupled plasma atomic emission spectrometry (ICP-AES). The fluorescence emission spectrum was recorded on a Hitachi 850 Fluorescence Spectrometer.

2.3. The preparation and photoelectrochemical measurements of lanthanide metal-ion-doped TiO_2 electrodes

The preparation of electrode was reported elsewhere [20]. In this work, the suspension of TiO_2 or metal-ion-doped TiO_2 with a concentration of 8.0 g dm^{-3} was dispersed ultrasonically before use. Four drops (ca. 0.2 ml) of the suspension were applied onto a piece of transparent conducting glass (2.0 cm $\times$ 1.8 cm, fluorine-doped SnO_2, 50 Ω sq^{-1}) which was heated on a warm plate, then the suspension was spread with a glass rod. The sample was sintered in N_2 at 480°C for 30 min, and than cooled to room temperature immediately. A layer of porous TiO_2 film formed on the conducting glass. The thickness of electrode films was measured with Tencor Alpha-Step Profiler.

The samples of different metal-ion-doped TiO_2 were designated as TM-X where T and M denote TiO_2 and the metal ion, respectively, and X is the initial dose of metal ion. For example, TEu-5 represents Eu^{3+}-doped TiO_2 containing 5% Eu^{3+}.

All photoelectrochemical measurements were carried out by using a standard three-electrode system equipped with a quartz window, a saturated calomel reference electrode (SCE) and a platinum wire counter-electrode placed in a separate compartment. A 0.1 mol dm^{-3} SCN^- solution (pH 4.0) was used as electrolyte. A Model 173 potentiostat was used for potentiostatic control and a Type 3036 X–Y Recorder was used for recording the photocurrent. All potentials reported were measured against SCE. The light source was a 200-W xenon lamp and the electrode was illuminated from front-side (the side of metal-ion-doped TiO_2 film).

2.4. The experiment of photocatalytic degradation of RB in lanthanide metal-ion-doped TiO_2 suspensions

All experiments of photocatalytic degradation were conducted in a photocatalytic reactor system containing two parts: a Pyrex glass tube (15 mm in diameter and 200 mm in length, containing a jacketed glass tube together with water circulation to avoid overheating) positioned parallel to the UV source, and a modified round-bottomed flask (500 ml) equipped with a magnetic stir bar. The two parts of the reactor were connected by Viton tubing and the contents circulated continuously with a peristaltic pump at a flow rate of 30 ml min^{-1}. The UV source was a 300 W-middle-pressure Hg lamp (100 mm long) with a maximum emission at approximately 365 nm.

In all experiments, 0.24 g samples (sintered at 480 C for 30 min) were dispersed in 300 ml deionized water, 3.00 ml RB solution of 1.0×10^{-3} mol l^{-1} was added to above suspension, then the pH of the suspension was adjusted with diluted HCl or KOH, and the samples were finally transferred to a round-bottomed flask. The suspension was purged with O_2 and stirred in the dark for 30 min to make the dye RB adsorption/desorption equilibrium on lanthanide metal-ion-doped TiO_2 nanoparti-

Table 1
The initial pH used for the precipitation of metal ions [21,22]

Metal ion	La^{3+}	Eu^{3+}	Pr^{3+}	Sm^{3+}	Nd^{3+}
pH	7.82	6.91	7.35	6.92	7.31

cles. During irradiation, the released CO_2 was absorbed with saturated solution of $Ba(OH)_2$ and the sample was taken at various intervals and centrifuged (10,000 rpm), we measured the change of absorbance spectrum and concentration of RB using UV–Vis Spectrometer (Shimuda 250 UV–Vis Spectrometer).

3. Results and discussion

3.1. XRD analysis

The XRD patterns showed that only anatase and brookite coexisted and no separate phase of metal oxide appeared in the samples of metal-ion-doped TiO_2 nanoparticles prepared at pH 1.8 and sintered at 480°C for 30 min. This can be explained from the initial pH used for the precipitation of metal ion and the free energy of formation for related oxide. Table 1 gives the initial pH used for the precipitation of several metal ions. It can be seen from Table 1 that the hydrolysis of these ions was difficult at pH 1.8.

3.2. TEM

The observation of TEM showed that the morphology and particle sizes ($\sim$ 10 nm) of metal-ion-doped TiO_2 were similar as undoped TiO_2 prepared at the same conditions (pH 1.8). The TEM paragraph is showed in Fig. 1.

3.3. The element analysis

The ICP analysis gave the content of metal ions in metal-ion-doped TiO_2 nanoparticles prepared at pH 1.8. Table 2 shows the analytical results which were in agreement with the results of XRD.

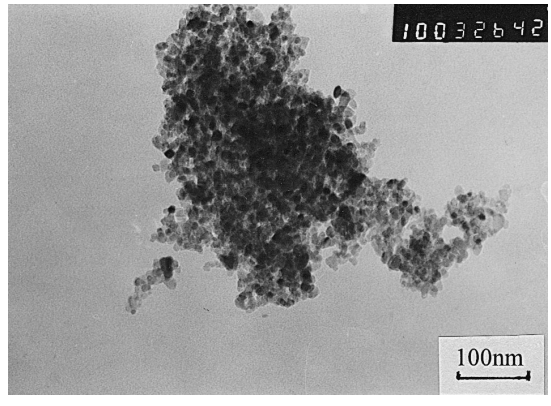

Fig. 1. The TEM photograph of Eu^{3+}-doped TiO_2 nanoparticles.

Table 2
The molar content of metal ions in metal-ion-doped TiO_2

Metal ions	La^{3+}	Eu^{3+}	Pr^{3+}	Sm^{3+}	Nd^{3+}
Content of ions (%)	0.55	1.10	0.31	0.10	0.30

3.4. Fluorescence emission spectra

The fluorescence spectra were measured for Eu^{3+}-doped TiO_2 before and after sintering at 480°C. It can be seen from Fig. 2 that the characteristic of Eu^{3+} emission spectrum appeared, peaked at 591.8 nm ($^5D_0 \rightarrow {}^7F_1$, magnetic dipole transition) and 616 nm ($^5D_0 \rightarrow {}^7F_2$, electronic dipole transition), respectively ($\lambda_{ex} = 265$ nm). This indicates that the efficient energy transfer took place between TiO_2 and Eu^{3+} ion. Fig. 2 also shows that the fluorescence intensity was higher for the sample after sintering than that before sintering, indicating that the content of Eu^{3+} ion in the lattice of TiO_2 nanoparticles after sintering was higher than that before sintering. It shows that the Eu^{3+} ions adsorbed on the surface of TiO_2 particles can enter into the lattice of TiO_2 though the process of sintering.

3.5. The photoelectrochemical properties of lanthanide metal-ion-doped TiO_2 electrodes

The photocurrent action spectra of six electrodes with a thickness of electrode film of 0.5 μm at the electrode potential of $+0.3$ V are shown in Fig. 3.

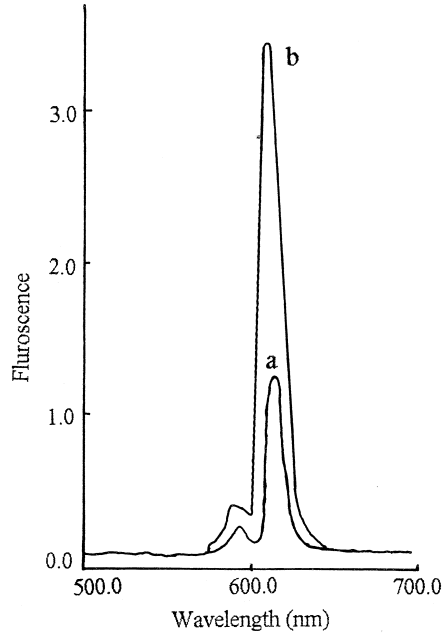

Fig. 2. The fluorescence emission spectra of Eu^{3+}-doped TiO_2 nanoparticles before (a) and after (b) sintering at 480°C.

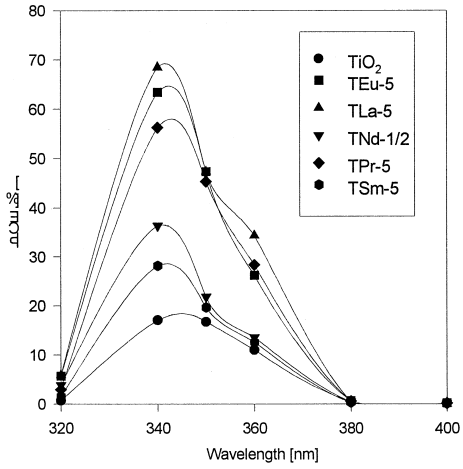

Fig. 3. The photocurrent action spectra of six electrodes.

The incident monochromatic photon to current conversion efficiency (IPCE), defined as the number of electrons generated by light in the external circuit divided by the number of incident photons, is plotted as a function of excitation wavelength. This was derived from the photocurrents by means of Eq. (1) [23,24]:

$$\mathrm{IPCE}(\%) = \frac{1.24 \times 10^3 \times i_{sc}\left(\mu\mathrm{A\,cm^{-2}}\right)}{\mathrm{Wavelength\,(nm)} \times \mathrm{Inc}\left(\mathrm{W\,m^{-2}}\right)} = \frac{1240 \times i_{sc}\left(\mu\mathrm{A\,cm^{-2}}\right)}{\mathrm{Wavelength\,(nm)} \times \mathrm{Inc}\left(\mu\mathrm{W\,cm^{-2}}\right)} \times 100, \tag{1}$$

where i_{sc} is photocurrent density, Inc is light intensity.

It can be seen that the IPCEs of TEu-5, TLa-5, TNd-5 and TPr-5 were much larger than that of undoped TiO_2, while the IPCE of TSm-5 was a little larger than that of undoped TiO_2, which indicates that the photogenerated electron-hole pairs were separated more efficiently in Eu^{3+}-, La^{3+}-, Nd^{3+}-, Pr^{3+}-doped TiO_2 nanoparticles.

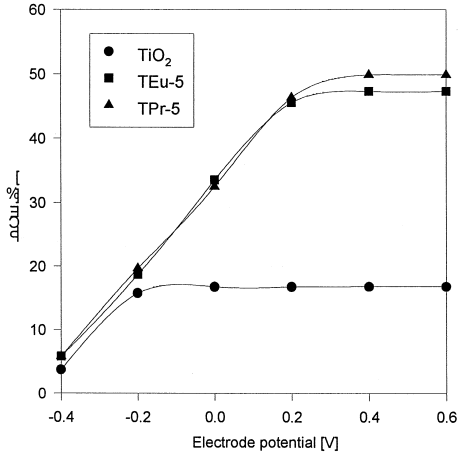

Fig. 4. The photocurrent–electrode potential curves for TiO_2 and TEu-5 and TPr-5 electrodes (light intensity at 350 nm, the area of electrode film is 0.5 cm^2).

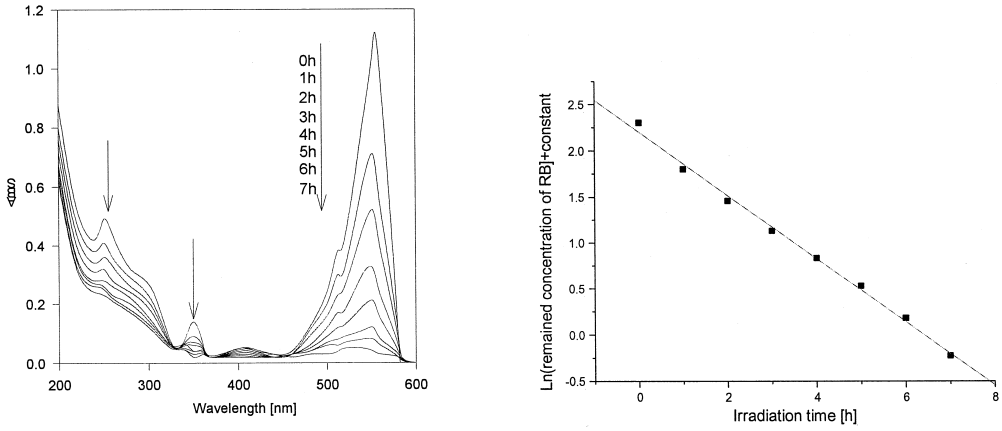

Fig. 5. (A) The change of absorption spectra of RB (1.0×10^{-5} mol dm^3) in the suspension of TiO_2 nanoparticles (1.0×10^{-3} mol dm^3, pH 6.0) under UV-light radiation in O_2 atmosphere with increasing irradiation time. (B) The curve of logarithm of the remaining concentration of RB ($\times 10^{-6}$ mol dm^3) during irradiation vs. irradiation time.

Fig. 4 shows the photocurrent–potential curves of TiO_2, TEu-5 and TPr-5 at the wavelength of 350 nm which also demonstrates the same tendency, i.e., the photocurrents of Eu^{3+}- and Pr^{3+}-doped TiO_2 nanocrystalline electrodes were much larger than that of undoped TiO_2 nanocrystalline electrode. Fig. 4 also shows that the photocurrents were very small at negative potential (-0.4 V), increased with increasing electrode potential, and then reached saturation at a certain potential. For undoped TiO_2 nanocrystalline electrodes, the photocurrent increased with electrode potential and reached saturation at -0.2 V, while for Eu^{3+}- and Pr^{3+}-doped TiO_2 nanocrystalline electrodes, the photocurrents increased with electrode potential but reached saturation at $+0.2$ V. But in the range of electrode potential from 0 to $+0.6$ V, the photocurrents of Eu^{3+}- and Pr^{3+}-doped TiO_2 electrodes were much larger than that of undoped TiO_2 electrode.

The actual doping concentration of lanthanide metal ions in TiO_2 is related to the ionic radii. The ionic radii of lanthanide ions (ca. 1.1 Å) were much larger than that of Ti^{4+} (0.60 Å), so lanthanide ions were difficult to enter into the lattice of TiO_2. The concentration of metal ions entered into the lattice of TiO_2 were very small.

For lanthanide ion-doped TiO_2 nanoparticles, the solid solution formed contained only a very low content of metal ions; a part of metal ions was adsorbed on the surface of TiO_2 particles. However, the low doping of lanthanide metal ions in TiO_2 may be in favor of the separation of electrons and holes, prolong the lifetime of carriers, reduce the recombination of electrons and holes, and finally make the photocurrent larger.

Table 3
The parameters of photocatalytic degradation of RB in the undoped TiO_2 nanoparticles at three different pH of media

Parameters (pH)	Reaction rate constant k (h^{-1})	Average initial rate r_{ini} ($\times 10^6$ mol/l h)	Percent of remaining RB after irradiation for 4 h (%)	Percent of remaining RB after irradiation for 5 h (%)
3.0	1/2.45	1.95	26	20
6.0	1/2.15	2.25	23	17
10.0	1/3.00	1.71	45	35

Table 4
The parameters of photocatalytic degradation of RB in lanthanide metal-ion-doped TiO_2 nanoparticles at pH 6.0 of media

Parameters (samples)	Reaction rate constant k (h^{-1})	Initiated rate r_{ini} ($\times 10^6$ mol/l h)	Percent of remaining RB after irradiation for 4 h (%)	Percent of remaining RB after irradiation for 5 h (%)
TiO_2	1/2.15	2.25	23	17
TEu-5	1/1.89	2.74	11	6.5
TLa-5	1/2.00	2.74	12	9
TNd-1/2	1/1.95	2.41	12	6.9
TPr-5	1/1.81	2.59	12	5
TSm-5	1/2.15	2.22	15.5	7

3.6. Photocatalytic degradation of RB in lanthanide metal-ion-doped TiO_2 suspensions

Zhao et al. have studied the mechanism of photocatalytic degradation of RB in TiO_2 suspension under N_2 and O_2 atmosphere. The purpose of this work is to investigate the ability of the lanthanide metal-ion-doped TiO_2 nanoparticles on photocatalytic degradation of RB and compare it with that of undoped TiO_2 nanoparticle, so the experiments were conducted in O_2 atmosphere.

First, the effects of the pH of media on the reactivity of photocatalytic degradation of RB in undoped TiO_2 suspension were studied. Fig. 5A shows the change of absorption spectrum of RB (1.0×10^{-5} mol dm^3) in the suspension of TiO_2 nanoparticles (1.0×10^{-3} mol dm^3, pH 6.0) under the UV light radiation in O_2 atmosphere, and Fig. 5B shows the curve of logarithm of the remaining concentration of RB during irradiation vs. irradiation time — it shows a very good linearity which indicates that the photocatalytic degradation was a first-order reaction. The released CO_2 during irradiation was absorbed with the saturated solution of $Ba(OH)_2$ and the precipitation of $Ba(CO_3)_2$ was detected. Table 3 gives the first-order reaction rate constant (k), average initial rate (r_{ini}, calculated when the reaction was carried out for 3 h) and the percent of remaining RB after irradiated for 4 and 5 h at three different pH of media; it can be seen that the photocatalytic reaction was carried out fastest at the pH 6.0, so all experiments below were conducted at pH 6.0. The result was attributed to the equilibrium of the number of surface hydroxyl and the amount of adsorbed RB on the surface of TiO_2 nanoparticles. In low pH, the number of surface hydroxyl groups was higher but the amount of adsorption of RB on TiO_2 surface was less because RB is a positively charged dye and TiO_2 nanoparticles are also positively charged at low pH (pH < 6.6) and repulsive to each other at low pH, so the reaction parameters were smaller at low pH. At high pH, although RB and TiO_2 nanopaticles

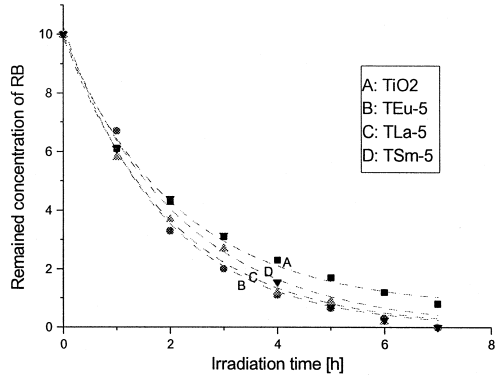

Fig. 6. The change of the concentration of RB with ($\times 10^{-6}$ mol dm^3) the irradiation time (the pH of media was 6.0).

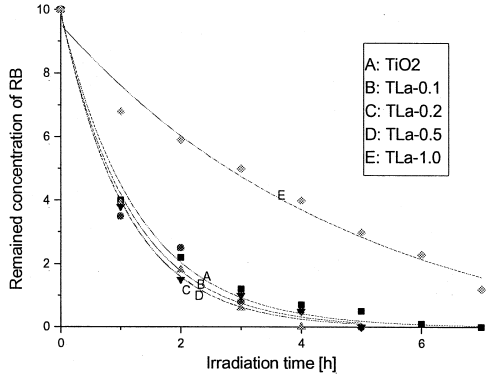

Fig. 7. The change of the concentration of RB ($\times 10^{-6}$ mol dm^3) during irradiation in La^{3+}-doped TiO_2 nanoparticles containing different La^{3+}.

attracted each other and the amount of adsorbed RB on TiO_2 nanoparticles was large, the number of surface hydroxyl of TiO_2 nanoparticles was small and the reaction parameters were also small at high pH. Therefore, there is an optimal pH to make the reaction parameters largest. The IR diffuse reflectance spectra of TiO_2 nanoparticles showed that the surface hydroxyl was more for samples treated at pH 3.0 than treated at pH 10.0.

Second, the reactivity of lanthanide metal-ion-doped TiO_2 nanoparticles to the photocatalytic degradation of RB was investigated. Table 4 gives the rate constant (k), average initial rate (r_{ini}) and the percent of remaining RB after irradiation for 4 and 5 h, and Fig. 6 shows the change of the concentration of RB with the irradiation time of three selected samples. It can been seen from Table 4 that the reaction rate constant (k) and average initial rate (r_{ini}) in Eu^{3+}-, La^{3+}-, Nd^{3+}- and Pr^{3+}-doped TiO_2 suspensions were larger than those in undoped TiO_2 suspension, but these parameters in Sm^{3+}-doped TiO_2 suspension were the same as those in undoped TiO_2 suspension. This result was similar with that of the measurement of photoelectrochemistry.

Finally, we investigate the effect of La^{3+} content in TiO_2 on the parameters of photocatalytic degradation of RB. Because the precipitated pH for lanthanide ions were larger (ca. pH 7.0), the samples were prepared at pH 7.0 and undoped TiO_2 was also prepared at pH 7.0 for comparison. Fig. 7 shows the change of the concentration of RB with irradiation time, and Table 5 shows the reaction parameters.

It can be seen by comparing Table 4 and Table 5 that reaction parameters (k, r_{ini}) in the presence of TiO_2 nanoparticles prepared at pH 7.0 were larger than those in the presence of TiO_2 nanoparticles prepared at pH 1.8, which is attributed to the difference of phase composition. Anatase and brookite co-existed in TiO_2 nanoparticles prepared at pH 1.8, but only anatase existed in TiO_2 nanoparticles

Table 5
The parameters of photocatalytic degradation of RB in La^{3+}-doped TiO_2 nanoparticles containing different La^{3+}

Parameters samples (% mol of La^{3+})	Reaction rate constant k (h^{-1})	Initial rate r_{ini} ($\times 10^6$ mol/l h)	Percent of remaining RB after irradiation for 4 h (%)	Percent of remaining RB after irradiation for 5 h (%)
0	1/1.270	2.82	7	5
0.1	1/1.163	2.93	7	0
0.2	1/1.088	3.03	0	0
0.5	1/1.088	2.93	0	0
1.0	1/4.911	1.44	55	50

prepared at pH 7.0; the photoresponse of TiO_2 nanocrystalline electrode prepared at pH 6.0 was higher than that prepared at pH 1.8 [19], so the photocatalytic ability of anatase was higher than that of the composite of anatase and brookite. Fig. 7 and Table 5 show that the k and r_{ini} values increased first with the increase of La^{3+} content, reached a maximum at the content of 0.2–0.5%, then decreased with the further increase of La^{3+} content. The change of k and r_{ini} with the different content of La^{3+} was shown in Fig. 8.

In the UV-light irradiation, the mechanism of photocatalytic degradation of dye is shown below.

$TiO_2 + h\nu \rightarrow TiO_2(e^-) + TiO_2(h^+)$	(1) The photogeneration of carriers.
$TiO_2(e^-) + O_2 \rightarrow O_2^-$	(2) The photogenerated electrons transfer to the surface of TiO_2 and are trapped by absorbed O_2.
$TiO_2(h^+) + OH \rightarrow OH\cdot$	(3) The photogenerated holes transfer to TiO_2 surface and are trapped by surface hydroxyl.
$TiO_2(e^-) + TiO_2(h^+) \rightarrow TiO_2$	(5) The recombination of photogenerated electrons and holes.
O_2^- or $OH\cdot$ + RB $\rightarrow \rightarrow \rightarrow \rightarrow CO_2$ et al.	(6) The photocatalytic degradation of RB.

The recombination of photogenerated carriers is the major factor to inhibit the IPCE and the reactivity of photocatalysis. As indicated in Section 1, the purpose of many research works is to decrease the recombination of carriers, prolong the lifetime of carriers, and improve the efficiency of separation of photogenerated carriers.

The maximum parameters (k and r_{ini}) at ca. 0.5% La^{3+} may be due to the fact that there is an optimal doping concentration of La^{3+} ions in TiO_2 nanoparticles for the most efficient separation of photogenerated electron-hole pairs. Pleskov [25] reported that the value of the space charge region potential for the efficient separation of electron-hole pairs must be not lower than 0.2 V. As the concentration of dopant ions increases, the surface barrier becomes higher and the space charge region narrower, the electron-hole pairs photogenerated within the region are efficiently separated by the large electric field before recombination. On the other hand, when the concentration of doping ions is high, the space charge region becomes very narrow and the penetration depth of light into TiO_2

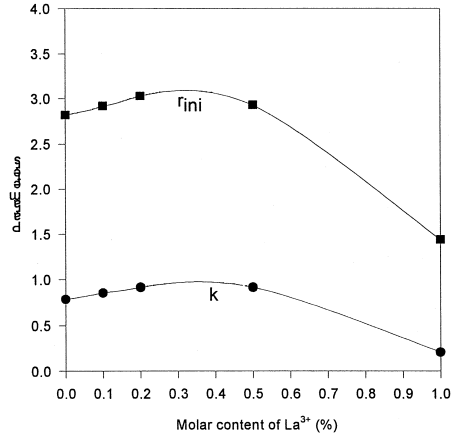

Fig. 8. The change of reaction parameters (k, r_{ini}) with the content of La^{3+} in La^{3+}-doped TiO_2 nanoparticles.

greatly exceeds the space charge layer, so the recombination of the photogenerated electron-hole pairs in semiconductor become easier. Consequently, there is an optimal concentration of dopant ions to make the thickness of space charge layer substantially equal to the light penetration depth. But for small colloidal particles, there is nearly no band-bending and the electrical field in colloidal semiconductors is usually small, so high dopant levels are favorable in producing a significant potential difference (permanent electric field) between the surface and the center of the particle to separate photogenerated electron-hole pairs efficiently [26].

4. Conclusion

The new type of photocatalyst of lanthanide metal-ion-doped TiO_2 nanoparticles was investigated in the paper with respect to its preparation, photoelectrochemical properties and the reactivity for photocatalytic degradation of dye RB. The results showed that the photogenerated carriers were separated efficiently in lanthanide metal-ion-doped TiO_2 nanoparticles, so the reactivity of the photocatalyst to the photodegradation of RB was high.

Acknowledgements

Support from the National Natural and Science Foundation of China (project number 29673003) and Doctoral Program Foundation of Higher Education is gratefully acknowledged.

References

[1] M.R. Hoffmann, S.T. Martin, W. Choi et al., Chem. Rev. 95 (1995) 69–76.
[2] R.W. Mattews, J. Chem. Soc. Faraday Trans. I 85 (6) (1989) 1291–1302.
[3] J.R. Darwent, A. Lepre, J. Chem. Soc. Faraday Trans. 2 82 (1986) 1457–1468.
[4] H. Al-Ekiabi, N. Serpone, E. Pelizzetti et al., Langmuir 5 (1989) 250–255.
[5] A. Sclafani, L. Palmisano, Solar Energy Mater. Solar Cells 51 (1998) 203–219.
[6] K. Vinodgopal, I. Bedja, P.V. Kamat, Chem. Mater. 8 (1996) 2180–2187.
[7] K.R. Gopidas, M. Bohorquez, P.V. Kamat, J. Phys. Chem. 94 6435.
[8] H.S. Zhou, I. Honma, H. Komiyama, J. Phys. Chem. 97 (1993) 895.
[9] S. Hotchandani, P.V. Kamat, J. Phys. Chem. 96 (1992) 6834.
[10] J. Rabani, J. Phys. Chem. 93 (1989) 7707.
[11] M. Ocana, W.P. Hsu, E. Matijevic, Langmuir 7 (1991) 2911.
[12] L. Palmisano, V. Augugliaro, A. Sclafani et al. 92 (1988) 6710–6713.
[13] J. Soria, J.C. Conesa, V. Augugliaro et al., J. Phys. Chem. 95 (1991) 274–282.
[14] Z. Luo, Q.-H Gao, J. Photochem. Photobiol. A: Chem. 63 (1992) 367.
[15] W. Choi, A. Termin, M.R. Hoffmann, J. Phys. Chem. 98 (1994) 13669–13679.
[16] F.L. Zhang, J.C. Zhao, L. Zang et al., J. Mol. Catal. A: Chem. 120 (1997) 173–178.
[17] P. Qu, J. Zhao, T. Shen, J. Mol. Catal. A: Chem. 129 (1998) 257–268.
[18] T.X. Wu, G.M. Liu, J.C. Zhao, J. Phys. Chem. B 102 (1998) 5845–5851.
[19] H.M. Cheng, J.M. Ma, Z.G. Zhao et al., Chem. Mater. 8 (1995) 895.
[20] Y.Q. Wang, H.M. Cheng, Y.Z. Hao et al., Preparation, J. Mater. Sci. (1999) in press.
[21] Inorgnic Chemistry People's Education, Shanghai, 1978.

[22] Svehla, Vogel's Textbook of Macro and Semimacro Qualitative Inorganic Analysis, 5th edn., 1978.
[23] M.K. Nazeeruddin, A. Kay, M. Gratzel, J. Am. Chem. Soc. 115 (1993) 6832.
[24] D. Liu, R.W. Fessenden, G.L. Hug, P.V. Kamat, J. Phys. Chem. B 101 (1997) 2590–2853.
[25] Y.V. Pleskov, Sov. Electrochem. 17 (1981) 1.
[26] A. Hagfeldt, M. Grätzel, Chem. Rev. 95 (1995) 49–68.